**Research & Reviews: Journal of Material Sciences**
DOI: 10.4172/2321-6212.1000177

e-ISSN: 2321-6212
p-ISSN: 2347-2278

# Silicon Carbide-Derived Carbon Coated Graphitized Mesocarbon Microbead Composites for Anode of Lithium-Ion Battery

**Zhengwei Cui[1], Ye Cong [1*], Xuelian Du[1], Xuanke Li[1,2], Jiang Zhang[1], Zhijun Dong[1], Guanming Yuan[1] and Yanjun Li[1]**

[1]Hubei Province Key Laboratory of Coal Conversion and New Carbon Materials, Wuhan University of Science and Technology, Wuhan, PR. China

[2]The State Key Laboratory of Refractories and Metallurgy, Wuhan University of Science and Technology, Wuhan, PR. China

## Research Article

Received: 16/06/2017
Accepted: 06/07/2017
Published: 10/07/2017

***For Correspondence**

Ye Cong, Hubei Province Key Laboratory of Coal Conversion and New Carbon Materials, Wuhan University of Science and Technology Wuhan, PR. China
Tel: +86-27-86556906

**Email:** congye626@126.com

**Keywords:** Silicon carbide-derived carbon, Composite, Anode, Lithium-ion battery

**ABSTRACT**

Unique silicon carbide-derived carbon (SiC-CDC) and graphitized mesocarbon microbead (GMCMB) composites (GMCMB@SiC-CDC) were prepared by solid reaction of GMCMB and silicon and following etching reaction with chlorine. The microstructure of SiC-CDC was characterized as mainly amorphous carbon combined with some short and curved sheets of graphite. N2 adsorption/desorption isotherms and pore size distributions proved the composites presented both an enormous amount micropores centered at around 0.5~0.6 nm and a few mesopores (2~50 nm). The GMCMB@SiC-CDC composites showed higher specific surface area and pore volume, especially the microporous surface area and volume. The composites as the anode materials manifested much higher charge specific capacities of 877.6 $mAh{\cdot}g^{-1}$ at the first cycle compared with pure GMCMB of 359.6 $mAh{\cdot}g^{-1}$, which was probable that Li ions could insert into not only carbon layers but also micropores. The GMCMB@SiC-CDC composites presented better discharge specific capacities at higher charge/discharge rates. The component and electrochemical performances of the composites can be optimized through changing the molar ratio of GMCMB/Si to control the corresponding proportion of SiC-CDC and GMCMB.

## INTRODUCTION

Li-ion battery (LIB) has been extensively used in portable electronics and electric vehicles due to its unique properties including high voltage, low discharge rate, small size and non-memory effect [1,2]. However, it is hard to meet the future requirements with high level performances of higher energy/power densities, excellent rate capability, long cycle life, environmental benignity and low cost [3,4]. Graphite is the traditional commercial anode material for LIBs in the last decades, which also suffers sever surface structure disordering upon prolonged cycling and lower rate capability [5,6].

Carbide-derived carbon (CDC) as a new type of carbon nanomaterials has attracted numerous attentions for the high purity, high specific surface area, tunable pore size, narrow pore size distribution and so on [7-10]. Their applications extend from gas storage and separation, catalyst support, electric double capacitors and Li-ion and Li-S battery [11-18]. CDCs commonly produced by selective extraction of the non-carbon components from carbides through leaching in supercritical water, high-temperature etching with halogens, vacuum decomposition and wet HF treatment. Etching with halogens at high-temperature is the most widely used approach to prepare CDCs due to its simple and economical process. The experimental conditions play critical roles on the carbon structure such as the carbide precursors, etching temperature and time, gas stream and so on. Taking the etching temperature as an example, amorphous structure of CDCs with uniform and relatively small pores would be produced at lower temperature, while partly graphitic ribbon structure of CDCs with less uniform and larger pores would be found at higher temperature. Nowadays, the applications of carbide-derived carbons mainly focus on gas storage and supercapacitors. But few researches on Li-ion batteries are explored. Yeon and co-workers reported that $B_4C$-CDC, $TiC_7N_3$-CDC and TiC-CDC with controllable pore textures and structures could be synthesized by chlorine treatment of the corresponding precursors ranged the temperature

e-ISSN: 2321-6212
p-ISSN: 2347-2278

from 600 to 1200°C. Both $B_4C$-CDC and $TiC_7N_3$-CDC exhibited higher discharge capacity and showed excellent potential as the anode materials of lithium battery [17]. Furthermore, Yeon et al. proposed that the post air-treatment at 550°C could increase mesoporisity of CDCs by removal of the amorphous phase and enlarger the interlayer distance, which may give rise to a notable synergistic effect on enhancement of discharge capacity during prolonged cycle. The discharge capacities of the air-treated CDCs as the anode material for lithium ion battery could reach 913 $mAh{\cdot}g^{-1}$ at the 220$^{th}$ cycle at 0.1 C [5]. It is probably an effective approach to improve the electrochemical performances by combining CDCs with other carbonaceous materials such as graphite to form heterojunction structure.

In this study, unique graphitized mesocarbon microbead and silicon carbide-derived carbon (GMCMB@SiC-CDC) composites were prepared by etching SiC coated graphitized mesocarbon microbead (GMCMB@SiC) precursors with chlorine at high temperature. The composites possessed characteristics of both graphitized carbon layers and abundant micro-porous carbide-derived carbons. Because the precursors of GMCMB@SiC were synthesized by reaction of GMCMB and silicon powder (Si), the pore structure and content of CDC in the composites can be controlled by changing the molar ratio of GMCMB/Si. The charge-discharge performances, cycling properties and rate performances of the composites as the anode materials for Li-ion batteries were investigated. Compared with pure GMCMB, the GMCMB@SiC-CDC composites presented better discharge specific capacities at higher charge/discharge rates.

## EXPERIMENTAL SECTION

### Peparation of GMCMB@ SiC-CDC Composites

Graphitized mesocarbon microbead (<20 μm) and silicon powder (~300 mesh and purity above 99.99%) were used as the raw materials and reacted in a horizontal tubular furnace under argon protection at 1600°C for 2 h. By varying the molar ratio of GMCMB/Si, silicon carbide coated GMCMB (GMCMB@SiC-R) were prepared, where R denoted as the molar of GMCMB/Si. Subsequently, the obtained GMCMB@SiC-R composites were placed into a quartz boat in a tubular furnace and raised the temperature by flushing with argon. After reaching the desired temperature (1000°C), the argon flow was replaced with high purity chlorine (99.999%) at a flow rate of 20~30 $mL{\cdot}min^{-1}$ for 1.5 h. After completion of etching reaction, the reactor was flushed with higher flow of argon (300 $mL{\cdot}min^{-1}$) to remove the residual chloride and then cooled down to room temperature. The obtained final products were denoted as GMCMB@SiC-CDC-R and simplified as GMCMB@CDC-R in the following figures and tables.

### Characterizations

X-ray diffraction (XRD) patterns were collected on Philips X Pert MPD Pro X-ray diffractometer with Cu Kα radiation (λ=1.54056 Å, 40 kV, 30 mA). The morphology of the composites was analyzed using a VEGE 3 SBH-EasyProbe scanning electron microscope. High-resolution transmission electron microscopy (HRTEM) was performed by a JEOL (JEM 2100) microscopy with an accelerating voltage at 200 kV. Raman spectra were recorded on a Renishaw in Via Reflex spectrometer with He-Ne laser (λ=632.8 nm) excitation. $N_2$ adsorption/desorption isotherms were carried out on a Micromeritics ASAP2020 analyzer at 77 K. The samples were degassed in vaccum at 623 K for 4 h before the measurement. The specific surface areas ($S_{BET}$) of the composites were calculated by the Brunauer-Emmett-Teller (BET) method from the nitrogen adsorption data in the relative pressure range ($P/P_0$) of 0.04~0.20. The total pore volume ($V_t$) was calculated the amount of $N_2$ uptake at relative pressure $P/P_0$=0.998. The pore size distributions were evaluated by the density functional theory (DFT) method according to the nitrogen adsorption isotherms, assuming a silt-shaped pore model.

### Preparation of Electrode and Electrochemical Measurements

Electrochemical measurements were performed using CR2016-type coin cells assembled in an argon-filled glove box. The prepared composites used as the active materials, conductive carbon black and polyvinylidene fluoride (PVDF) as a binder were homogeneously mixed in N-methyl pyrolidinone (NMP) at a weight ratio of 80:10:10. The slurry was deposited onto a copper foil and dried under vacuum at 60°C overnight. The working electrode and lithium foil as the counter electrode were assembled into cells with 1 M $LiPF_6$ solution in ethylene carbonate (EC)/dimethyl carbonate (DMC)/ethyl methyl carbonate (EMC) (EC:DMC:EMC=1:1:1, v/v/v) as the electrolyte and Celgard 2325 as the separator. The electrochemical performance was tested by galvanostatic charge–discharge experiments in the potential range of 0.005~2.000 V (vs. $Li/Li^+$) on a LAND-CT 2001A battery test system.

## RESULTS AND DISCUSSION

The XRD patterns of GMCMB@SiC prepared with different molar ratios of GMCMB/Si are shown in **Figure 1**. Two peaks centered at 2θ=26.6°, 54.8° are contributed to the (002) and (004) crystal plane of carbon (GMCMB), respectively. And there are five sharp peaks at about 2θ=35.7°, 41.5°, 60.1°, 71.9°, 75.7°, corresponding to diffractions from the (111), (200), (220), (311), (222) crystal planes of a face-centered cubic phase SiC. It can be clearly seen that the intensities of the diffraction peaks attributed to the SiC show a significant increase as the molar ratio of GMCMB/Si decreases. It indicates that the content of SiC in the GMCMB@SiC composites increases and the content of GMCMB decreases since GMCMB are used as a sacrificed template to react with silicon. Two weak peaks ascribed to silicon can be observed in **Figure 1a**, which is due to the incompletely reactive silicon as the molar ratio of 1. Therefore, the reaction depth can be effectively controlled by varying the molar ratio of GMCMB/Si. Consequently, the thickness of SiC as out-shell and the size of GMCMB as inner-core in the composites can be adjusted effectively.

**Research & Reviews: Journal of Material Sciences**
DOI: 10.4172/2321-6212.1000177
e-ISSN: 2321-6212
p-ISSN: 2347-2278

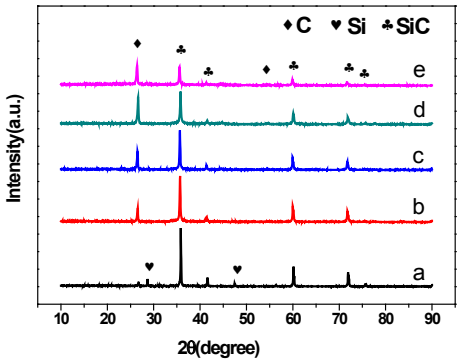


**Figure 1.** XRD patterns of GMCMB@SiC prepared with different molar ratios of GMCMB/Si. (a) 1; (b) 2; (c) 3; (d) 4; (e) 5

After chlorination (shown in **Figure 2**), the peaks ascribed to the cubic phase SiC have disappeared except for GMCMB@SiC-CDC-1, which is due to its much higher content of SiC. It can be completely etched using higher chlorination temperature or longer chlorination time. The residual diffraction peaks at 2θ=26.5, 42.4, 44.6, 54.7 are attributed to the crystal planes of (002), (100), (101), (004) of carbon, which indicates that the products are mainly composed of carbon. In addition, the diffraction intensities increase with the decrease of the molar ratios of GMCMB/Si, The results are coincident with that of **Figure 1**.

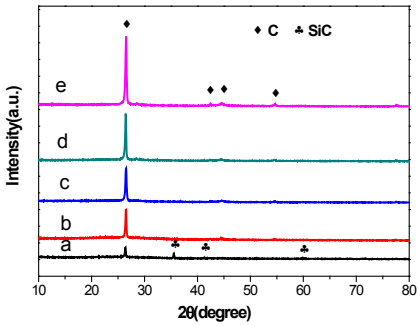


**Figure 2.** XRD patterns of GMCMB@SiC-CDC composites etched at 1000°C for 1.5 h with different GMCMB/Si molar ratios (a) 1; (b) 2; (c) 3; (d) 4; (e) 5

**Figure 3** displays the SEM images of GMCMB raw material, GMCMB@SiC-2 before and after chlorination at 1000°C, respectively. It is obvious that the surface roughness of GMCMB@SiC-2 increases compared to the raw materials and fine particles cover on the surface. After chlorination, the composites still keep the sphere-like shape similar with the pristine GMCMB. But the surface is growing porous and loose.

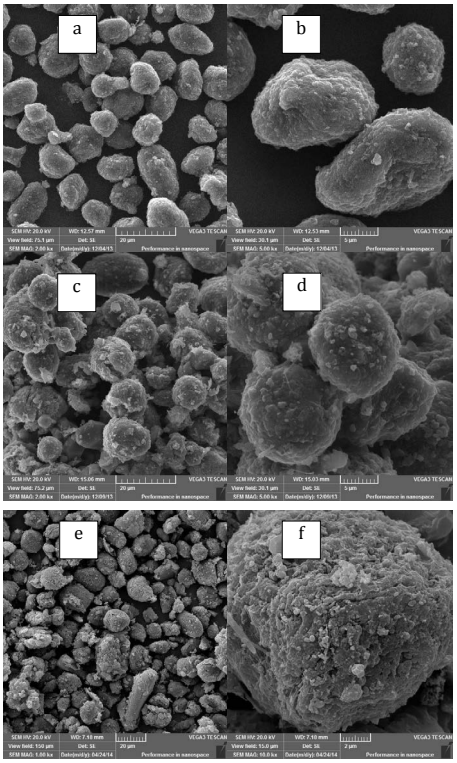


**Figure 3.** SEM images of (a, b) GMCMB; (c, d) GMCMB@SiC-2; (e, f) GMCMB@SiC-CDC-2

**Research & Reviews: Journal of Material Sciences**
DOI: 10.4172/2321-6212.1000177
e-ISSN: 2321-6212
p-ISSN: 2347-2278

Raman spectroscopy is a unique technique to analyze the characteristics of carbon materials. The Raman spectra of GMCMB and the synthesized GMCMB@SiC-CDC-2 are shown in **Figure 4**. GMCMB exhibits a sharp and strong peak at ~1582 $cm^{-1}$, which is labeled as G band. The G band is corresponding to the in-plane vibration of $sp^2$ bonded carbon atoms with $E_{2g}$ symmetry (so-called order mode). A lower intensity peak at ~1335 $cm^{-1}$ of *D* band suggests the presence of $sp^3$ defects in graphite such as bond-angle disorder, bond-length disorder, vacancies, and edge defects (so-called disorder mode) [19-21]. The second-order peak of D band (2D) at ~2667 $cm^{-1}$ shows higher intensity and symmetry, which is related with the crystallographic ordering of the graphitic structure [19]. In comparison with GMCMB, GMCMB@SiC-CDC-2 presents wider and stronger D band and the ratio of D band and G band intensities ($I_D/I_G$) increase extensively. It suggests the formed CDC in the composites is mainly amorphous [22].

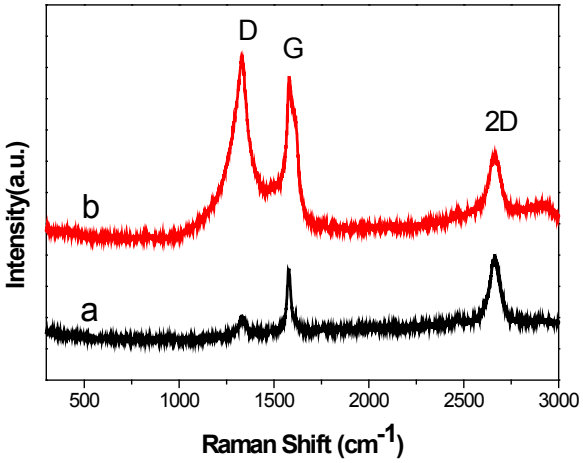


**Figure 4.** Raman spectra of (a) GMCMB and (b) GMCMB@SiC-CDC-2

The microstructure at the atomic scale of GMCMB/SiC-2 before and after chlorination at 1000°C for 1.5 h are revealed by high-resolution transmission electron microscopy (HRTEM). Distinct differences can be found in **Figure 5**. As seen from the high magnification image (**Figure 5a**), legible lattice fringes can be observed. The lattice fringe space is 0.217 nm, which is corresponding to the (200) crystal planes of cubic β-SiC. The result indicates the product synthesized by solid phase reaction under high temperature possesses well-developed cubic SiC phase, which agrees with the results of XRD. After chlorination, the lattice fringes disappear and the microstructure of SiC-CDC is mainly comprised of amorphous carbon with some short and curved sheets of graphite. The image of SiC-CDC shows a typical disordered carbon with some porosity.

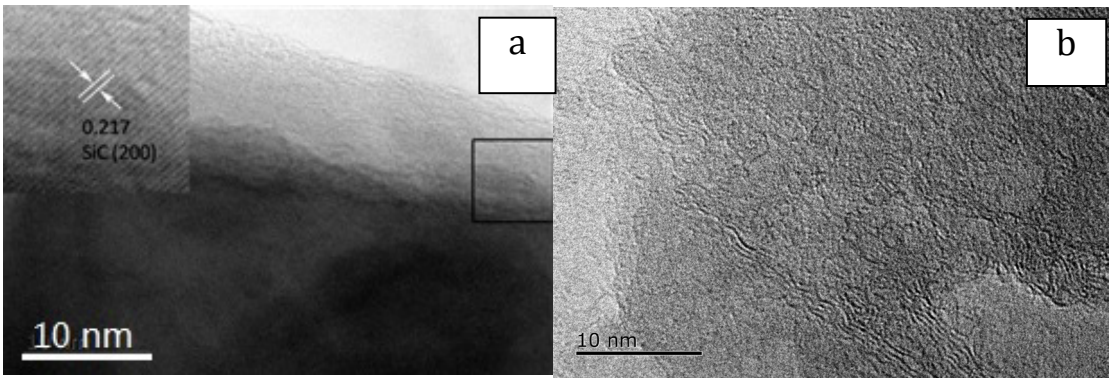


**Figure 5.** HRTEM images of GMCMB@SiC-2 (a) before and (b) after chlorination at 1000°C

**Figure 6a** shows the $N_2$ adsorption/desorption isotherms of GMCMB@SiC-CDC-*R* chlorinated at 1000°C for 1.5 h. All samples exhibit large adsorbed quantity at relatively low pressure ($P/P_0$<0.1), which is assigned to a typical I-type isotherm according to IUPAC classification [23]. This means the pores in the prepared composites are mainly micropores (< 2 nm) generated by removing Si atoms from SiC lattice [24,25]. In addition, the adsorbed quantity gradually increases with the decrease of GMCMB/Si molar ratio, which is due to the increasing content of SiC-CDC in the composites. The isotherms also exhibit a weak hysteresis loop located at the relative high pressure ($P/P_0$>0.4), indicating the presence of mesopores (>2 nm) formed between graphitic ribbons [10]. The pore size distributions calculated by DFT method are presented in **Figure 6b**. All GMCMB@SiC-CDC-*R* exhibit narrow peaks centered at around 0.5~0.6 nm, which is typical pore size of carbide derived carbons [26]. **Table 1** lists the porosity parameters and the specific surface area, pore volume and the centered micropore size derived from DFT model. Comparing with the sample before chlorination, the GMCMB@SiC-CDC composites show higher specific surface area and pore volume, especially the microporous surface area and volume. Both $S_{BET}$ and $S_{micro}$ increase with decrease molar ratio of GMCMB/Si and $S_{BET}$ is mainly contributed by microporous.

**Research & Reviews: Journal of Material Sciences**
DOI: 10.4172/2321-6212.1000177
e-ISSN: 2321-6212
p-ISSN: 2347-2278

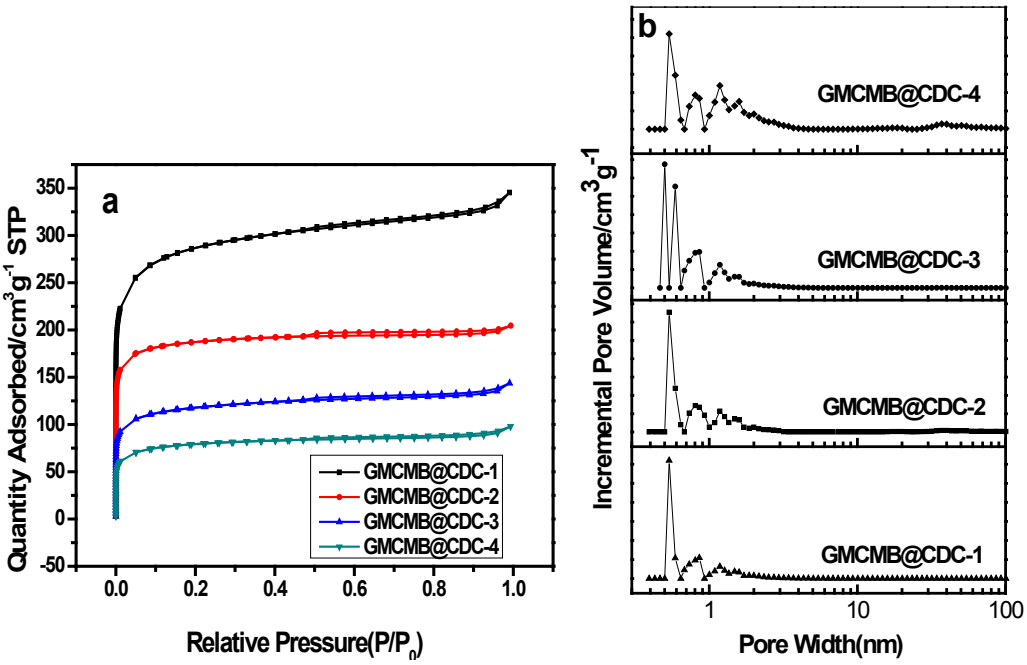


**Figure 6.** (a) $N_2$ adsorption/desorption isotherms at 77 K and (b) pore size distributions of GMCMB@SiC-CDC composites with different GMCMB/Si molar ratios

**Table 1**. Porosity parameters of GMCMB@SiC-CDC composites

| Sample | $S_{BET}$/$m^2 \cdot g^{-1}$ | $S_{micro}$/$m^2 \cdot g^{-1}$ | $V_{total}$/$cm^3 \cdot g^{-1}$ | $V_{micro}$/$cm^3 \cdot g^{-1}$ | Micropore size/nm |
|---|---|---|---|---|---|
| GMCMB@SiC-2 | 0.4 | ~0 | ~0 | ~0 | - |
| GMCMB@CDC-1 | 1050.8 | 744.1 | 0.534 | 0.308 | 0.58 |
| GMCMB@CDC-2 | 710.7 | 604.8 | 0.316 | 0.242 | 0.57 |
| GMCMB@CDC-3 | 440.3 | 325.3 | 0.222 | 0.131 | 0.59 |
| GMCMB@CDC-4 | 291.8 | 214.2 | 0.151 | 0.088 | 0.60 |

One of the most potential applications of the GMCMB@ SiC-CDC composites is used as the anode materials of Li ion batteries. The electrochemical performances toward Li insertion/extraction were investigated. The galvanostatic charge/discharge voltage profiles of the first cycle at 0.1C in the voltage range of 0.005~2.000 V vs Li+/Li are shown in **Figure 7a**. The GMCMB@SiC-CDC composites present identically different charge and discharge shape compared with GMCMB. The plateau in the voltage range of 0.75~0.25 V vs Li+/Li is attributed to the formation of a solid electrolyte interphase (SEI) layer and to an irreversible reaction with the electrode materials by consuming Li ions. The plateaus of GMCMB@ SiC-CDC-*R* are longer than that of GMCMB, which is due to their larger specific surface areas and higher consumption of Li ions to form SEI layer. The other plateau below 0.25 V vs Li+/Li results from lithium insertion and extraction in the carbon layers of the residual GMCMB.

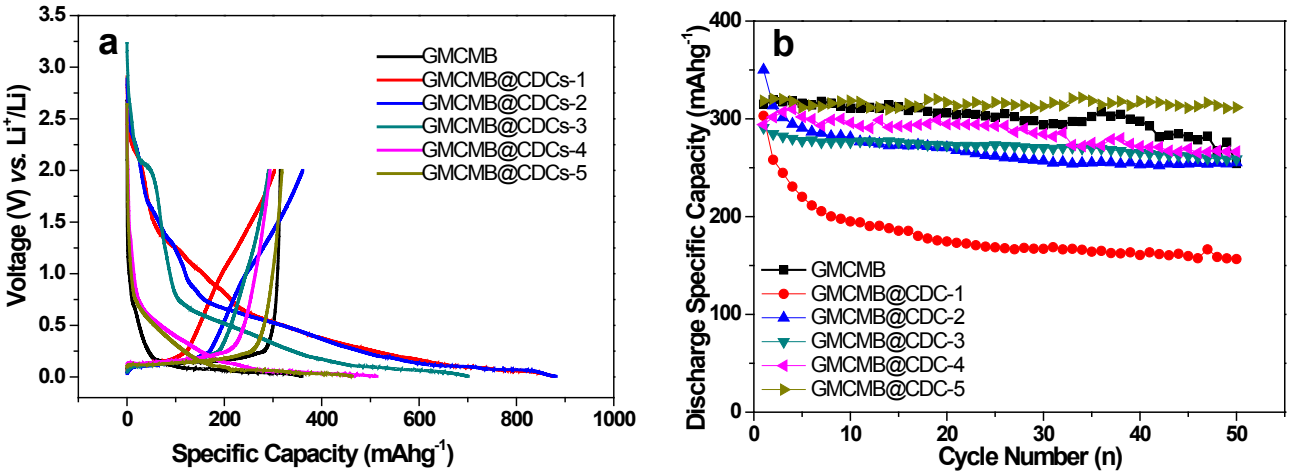


**Figure 7.** (a) Galvanostatic charge/discharge voltage profiles of the first cycle and (b) cycling performances of GMCMB and GMCMB@SiC-CDC-*R* at 0.1C

Research & Reviews: Journal of Material Sciences
DOI: 10.4172/2321-6212.1000177
e-ISSN: 2321-6212
p-ISSN: 2347-2278

**Table 2.** The charge/discharge characteristics of GMCMB and GMCMB@SiC-CDC composites

| Samples | First charge capacity/ ($mAh·g^{-1}$) | First discharge capacity/($mAh·g^{-1}$) | First columbic efficiency/% | Capacity retention after 50 cycles/% |
|---|---|---|---|---|
| GMCMB | 359.6 | 314.9 | 87.6 | 80.7 |
| GMCMB@CDC-1 | 877.6 | 303.1 | 34.5 | 51.7 |
| GMCMB@CDC-2 | 874.2 | 350.1 | 40.1 | 72.9 |
| GMCMB@CDC-3 | 700.9 | 290.9 | 41.5 | 89.0 |
| GMCMB@CDC-4 | 513.5 | 294.1 | 57.3 | 90.5 |
| GMCMB@CDC-5 | 462.7 | 318.5 | 68.8 | 96.9 |

The prepared GMCMB@ SiC-CDC composites show much higher charge capacity than GMCMB in the first cycle (list in **Table 2**), because the pores in the carbide derived carbon would contribute to the charge of lithium species. The voltage hysteresis between the charge and discharge curve is observed for the prepared GMCMB@SiC-CDC composites. It is probable that Li ions insert into not only carbon layers but also micropores during the charge process. There are defects structure and radical carbon atoms, which possess stronger interaction with Li ions. Therefore, Li ions need higher voltage to break away from the micropores and accomplish the delithiation process. In addition, the irreversible capacity loss increases and the first columbic efficiency decrease with the decline of the molar ratio of GMCMB/Si. It is reasonable that the corresponding surface area increases and the consumption of Li ions to form SEI layer also increases. Meanwhile, part of Li ions insertion into the micropores may be remained and results in the slow extraction speed of Li ions from the micropores. It should be noted that the discharge profiles of the GMCMB@SiC-CDC composites are steep and the composites may obtain much higher discharge capacity at higher voltage.

The cycling performances of GMCMB and GMCMB@ SiC-CDC composites are presented in **Figure 7b**. The specific capacities of the prepared GMCMB@CDC composites have basically stabilized after 10 cycles except for GMCMB@CDC-1 because of its highest micropore content. As compared to GMCMB, GMCMB@ SiC-CDC-1 shows the highest specific capacities of 311.6 $mAhg^{-1}$ after 50 cycles, and presents the highest charge and discharge capacity retention rate of 96.9%, which are higher than that of GMCMB 254.2 and 80.7%. The reason is that the porous SiC-CDC layer covering on GMCMB can effectively depress the exfoliation of graphite layers caused by co-intercalation of solvent molecules and solvated lithium ions. However, excessively thick coatings of SiC-CDC will consume much more lithium ions to form SEI layer and cause a considerable reduction in specific capacity and capacity retention rate. So the materials should be optimized through changing the molar ratio of GMCMB/Si and controlling the shell thickness to obtain the optimum electrochemical performance.

The specific capacities of GMCMB and GMCMB@SiC-CDC-*R* at different charge/discharge rates are shown in **Figure 8**. It is obvious that GMCMB@SiC-CDC composites with higher molar ratio of GMCMB/Si manifest higher discharge specific capacities; while GMCMB@SiC-CDC composites with lower molar ratio of GMCMB/Si show better performance at higher charge/discharge rates. GMCMB@CDC-2 provides three times specific capacity at 2C compared with GMCMB. It is deduced that lithium ions can insert into both graphite carbon layers of GMCMB and nano-micropores of carbide derived carbons. The proper content of SiC-CDC facilitates improving not only the specific capacity but also the rate performance.

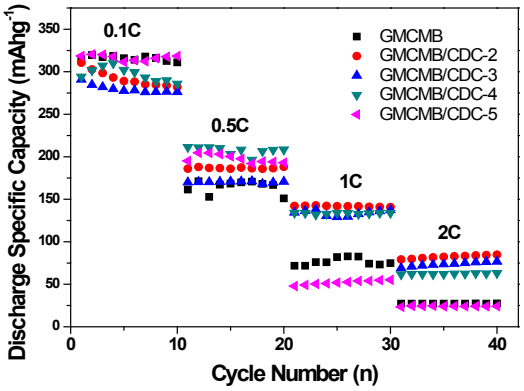


**Figure 8.** Specific capacity of GMCMB and GMCMB@CDC composites at different charge/discharge rates

## CONCLUSION

GMCMB@SiC-CDC composites with porous silicon carbide-derived carbon as the shell and graphitized MCMB as the core were prepared by etching the precursor of GMCMB@SiC. The relative proportion of two structural carbon, namely SiC-CDC and GMCMB, can be controlled by varying the molar ratio of GMCMB/Si in the synthesis of the GMCMB@SiC precursor. The prepared composites possess large quantities of micropores centered at around 0.5~0.6 and a few mesopores, giving rise to higher specific surface area and pore volume. The microstructure of SiC-CDC manifests typically amorphous carbon combined with short and curved sheets of graphite. The unique characteristics of the two-phase carbon composites are ascribed to improve the electrochemical performances especially the discharge specific capacities at higher charge/discharge rates.

e-ISSN: 2321-6212
p-ISSN: 2347-2278

## ACKNOWLEDGEMENTS

This research is financially supported by the National Natural Science Foundation of China (51472186, 51402221).

## REFERENCES

1. Yan L, et al. Ultrafine $TiO_2$ nanoparticles on reduced graphene oxide as anode materials for lithium ion batteries. Appl Mater Today 2017;8:31-34.
2. Ma H, et al. Carbon nanocages@ultrathin carbon nanosheets: One-step facile synthesis and application as anode material for lithium-ion batteries. Carbon 2016;105:586-592.
3. Zhang M, et al. Three-dimensional tungsten nitride nanowires as high performance anode material for lithium ion batteries. J Power Sources 2016;322:163-168.
4. Sagara RUR, et al. High capacity retention anode material for lithium ion battery, Electrochim Acta 2016;211:156-163.
5. Yeon S-H, et al. Unique cyclic performance of post-treated carbide-derived carbon as an anode electrode. Carbon 2014;78:91-101.
6. Beguin F, et al. A better understanding of the irreversible lighium insertion mechanisms in disordered cabons. J Phys Chem Solids 2004;65:211-217.
7. Yeon S-H, et al. High microporosity of carbide-derived carbon prepared from a vacuum-treated precursor for energy storage devices. Carbon 2017;118:327-338.
8. Yan P, et al. Structure and supercapacitive performance of hierarchical porous carbon obtained by catalyzing microporous carbide-derived carbon. Mater Lett 2015;139:340-343.
9. Presser V, et al. Carbide-derived carbons – from porous networks to nanotubes and graphene. Adv Func Mater 2011;21:810-833.
10. González-García P, et al. Nanostructure, porosity and electrochemical performance of chromium carbide derived carbons. Carbon 2015;85:38-49.
11. Oschatz M, et al. Carbide-derived carbon monoliths with hierarchical pore architectures. Angew Chem Int Ed 2012;51:7577-7580.
12. Oschatz M, et al. A cubic ordered, mesoporous carbide-derived carbon for gas and energy storage applications. Carbon 2010;48:3987-3992.
13. Borchardt L, et al. Transition metal loaded silicon carbide-derived carbons with enhanced catalytic properties. Carbon 2012;50:1861-1870.
14. Wu C, et al. Preparation and supercapacitive behaviors of the ordered mesoporous/microporous chromium carbide-derived carbons. J Power Sources 2014;269:818-824.
15. Yan P, et al. High-power supercapacitors based on hierarchical porous nanometer-sized silicon carbide-derived carbon. Electrochim Acta 2016;189:16-21.
16. Dyatkin B, et al. High capacitance of coarse-grained carbide derived carbon electrodes. J Power Sources 2016;306:32-41.
17. Yeon S-H, et al. Electrochemical performance of carbide-derived carbon anodes for lithium-ion batteries. J Phys Chem Solids 2013;74:1045-1055.
18. Wei Y, et al. Layered carbide-derived carbon with hierarchically porous structure for high rate lithium-sulfur batteries. Electrochim Acta 2016;188:385-392.
19. Wang H, et al. Adsorption and desorption of small molecule volatile organic compounds over carbide-derived carbon. Carbon 2014;67:712-720.
20. Becker P, et al. Chlorination of titanium carbide for the processing of nanoporous carbon: a kinetic study. Chem Eng J 2010;159:236-241.
21. Zhao Y, et al. Titanium carbide derived nanoporous carbon for supercapacitor applications. Int J Hydrogen Energ 2012;37:19395-19400.
22. Chmiola J, et al. Taberna. Anomalous increase in carbon capacitance at pore sizes less than 1 nanometer. Science 2006;313:1760-1763.
23. Casco ME, et al. Effect of the porous structure in carbon materials for $CO_2$ capture at atmospheric and high-pressure. Carbon 2014;67:230-235.
24. Wei Y, et al. Layered carbide-derived carbon with hierarchically porous structure for high rate lithium-sulfur batteries. Electrochim Acta 2016;188:385-392.
25. Zhou DD, et al. Ordered hierarchical mesoporous/microporous carbon with optimized pore structure for supercapacitors. J Mater Chem A 2013;1:1192-1200.
26. Dyatkin B, et al. Capacitance, charge dynamics, and electrolyte-surface interactions in functionalized carbide-derived carbon electrodes. Prog Nat Sci: Mater Int 2015;25:631-641.